Tidal Diffusivity: A Mechanism for Frontogenesis*

HSIEN-WANG OU, CHANG-MING DONG, AND DAKE CHEN

Lamont-Doherty Earth Observatory, Columbia University, Palisades, New York

(Manuscript received 25 April 2001, in final form 7 October 2002)

ABSTRACT

It is hypothesized that tidal mixing may provide a ''diffusivity'' mechanism for frontogenesis. It stems from the fact that tidal diffusivity varies in the opposite sense from the water depth, so the vertically integrated diffusivity may exhibit a minimum at midshelf, thus giving rise to a maximum in the property gradient—even in the absence of flow convergence. An analytical model assuming a tidal diffusivity dominated by shear dispersion is used to elucidate the mechanism, which shows additionally that the front is located at a water depth that is about twice the tidal frictional depth—a prediction not inconsistent with some observed fronts. The proposed frontogenesis is demonstrated by numerical calculations using the Princeton Ocean Model (POM), which show the emergence of a front from an initial field of uniform gradient after tides are switched on, and the diagnosis of the numerical solution and its parameter dependence has corroborated the analytical model. It is suggested moreover that this diffusivity mechanism may be extended to the wind-induced mixing to explain the shelfbreak front off of the northeastern United States.

1. Introduction

There are two basic types of tidal fronts (Hill and Simpson 1989), as illustrated by the density field shown in Fig.1. Type I front is particularly prominent in winter when tidal mixing and surface cooling have rendered the shelf water vertically homogeneous; but primarily because of the salinity contrast between the coastal and offshore water, there exists a density front in midshelf that extends from the bottom to the surface. Besides the area around the British Isles (Hill and Simpson 1989), type I fronts are also observed in the eastern China seas (Hickox et al. 2000) and off the northeastern United States (Ullman and Cornillon 2001). Although their salinity contrast is derived from freshwater discharge, type I fronts should be distinguished from the more localized fronts marking the boundary of the river plume (Garvine 1995) or the fronts straddling the shelf break (Beardsley et al. 1985), for which tidal mixing is not of primary importance.

In summer, surface heating produces a seasonal thermocline offshore, which may not overcome the tidal mixing of the nearshore water that keeps it homogenized; the seasonal pycnocline thus would branch ashore to intersect both the bottom and surface, giving rise to the type II front. The lower branch retains the salinity signature of the type I front, while the upper branch marks the inshore boundary of the warm surface water. Perhaps due to its stronger density signature, the type II front has received much wider coverage in the literature.

Since the type II front represents the transition where the surface heating is just enough to overcome the tidal mixing, Simpson and Hunter (1974) proposed a criterion for its location based on the mechanical energy balance, which has received some observational support (Fedorov 1983). Such mechanical energy balance however bears no relevance to the occurrence of the type I front, which is particularly prominent in winter when there is no surface heating and the density lines are largely vertical. Although topographic steering of the type I front has been suspected (Hill and Simpson 1989), there are as yet no dynamical theories for its genesis.

In the larger context beyond tidal fronts, there is an extensive literature on frontogenesis given the ubiquitous nature of the phenomenon in both atmosphere and ocean. Most mechanisms invoke some kind of deformation fields, which may sharpen the property gradient where there is flow convergence (Hoskins and Bretherton 1972; Fedorov 1983; Ou 1984). Since the type I front typically contains little vertical and alongshore structure, mass continuity seems to preclude flow convergence as a significant factor. On the other hand, given the prominence of tides where the fronts are observed, one naturally seek their explanation through spatial inhomogeneity in the tidal mixing.

The efficiency of such mixing can be gauged by tidal diffusivity, a property widely used in the study of tidal

* Lamont-Doherty Earth Observatory Contribution Number 6388.

Corresponding author address: Dr. Hsien-Wang Ou, Lamont-Doherty Earth Observatory, Columbia University, Palisades, NY 10964. E-mail: dou@ldeo.columbia.edu

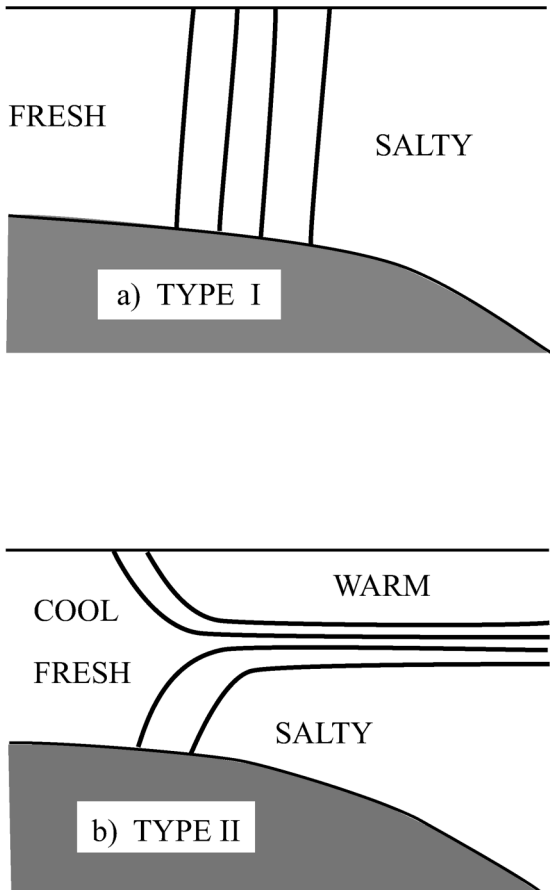

FIG. 1. Density fields for the two types of tidal fronts: (a) Type I front is present in winter and marks the offshore boundary of the low-salinity nearshore water, and (b) type II front is present in summer and represents the shoreward branching of the seasonal pycnocline as the nearshore water remains vertically mixed.

dispersion of tracers (Fisher et al. 1979). It is well known that such diffusivity arising from the vertical-shear dispersion can be several orders of magnitude greater than that associated with small-scale turbulence (Taylor 1953), and is needed to account for the observed dispersion (Geyer and Signell 1992). In fact, in regions where the dispersion is particularly rapid, additional effects of lateral-shear dispersion and tidal random walk need to be invoked to augment the tidal diffusivity (Zimmerman 1986).

Whereas the aforementioned studies are concerned with the time evolution of tracer patches, we apply the concept of tidal diffusivity here to the steady-state density field in the presence of a coastal buoyancy source. And in so doing, we find that the spatial variation of the tidal diffusivity associated with the depth change may yield a local maximum in the density gradient, thus providing a robust ''diffusivity'' mechanism for frontogenesis.

The paper is organized as follows. In section 2, we derive the equation governing the mean property field, based on which we propose in section 3 the diffusivity mechanism for frontogenesis. In section 4, we discuss the spatial variation of the tidal diffusivity that underlies the mechanism. In section 5, we present the analytical solution to illustrate the mechanism and to compare the model prediction with observations. In section 6, numerical calculations from the primitive equation Princeton Ocean Model (POM) are used to demonstrate the frontogenesis and to corroborate the analytical model. In section 7, we summarize the main findings and provide additional discussion.

2. Analytical model

The model domain is shown in Fig. 2 and consists of a cross-shore section of exponential bottom that is unvarying in the alongshore direction. A right-handed Cartesian coordinate system is used, with x and z axes directed offshore and upward respectively, and the origin set at the mean sea level where the water depth equals the tidal frictional depth (defined later). To isolate the tidal effect, we set the buoyancy flux through the surface to be zero and, since we are concerned with the type I front, we assume the vertical mixing to be sufficiently vigorous and/or density gradient sufficiently weak that the mean density lines are approximately vertical. The model is forced by tides, a coastal buoyancy source, and an offshore mass flux, as discussed next.

For simplicity, we assume that the tidal mixing is dominated by the cross-shore tidal motion and, on account of its slowness compared with the gravity wave propagation, its volume flux has a uniform amplitude in x, which defines the tidal forcing. A coastal buoyancy source is represented by a specified density deficit relative to the far field; and a small offshore mass flux, say, due to river discharge, is included to remove an unrealistic feature of the analytical solution, which however has little effect on the tidal front.

We first consider the mass balance in the tidal regime. The following steps are elementary, but are included to aid the later derivation of the density equation. We begin with the continuity equation

$$u_x + w_z = 0, \tag{2.1}$$

where the subscripts indicate partial derivatives. If one integrates this equation from the bottom (of depth h) to the free surface (of height η) and employs the kinematic boundary conditions, one obtains

$$\partial_x \int_{-h}^{\eta} u\, dz + \eta_t = 0, \tag{2.2}$$

which links the surface displacement to the divergence of the mass flux. Averaging (2.2) over the tidal period yields

$$\partial_x \left[\int_{-h}^{0} \overline{u}\, dz + (\overline{u'\eta'})_0 \right] = 0 \tag{2.3}$$

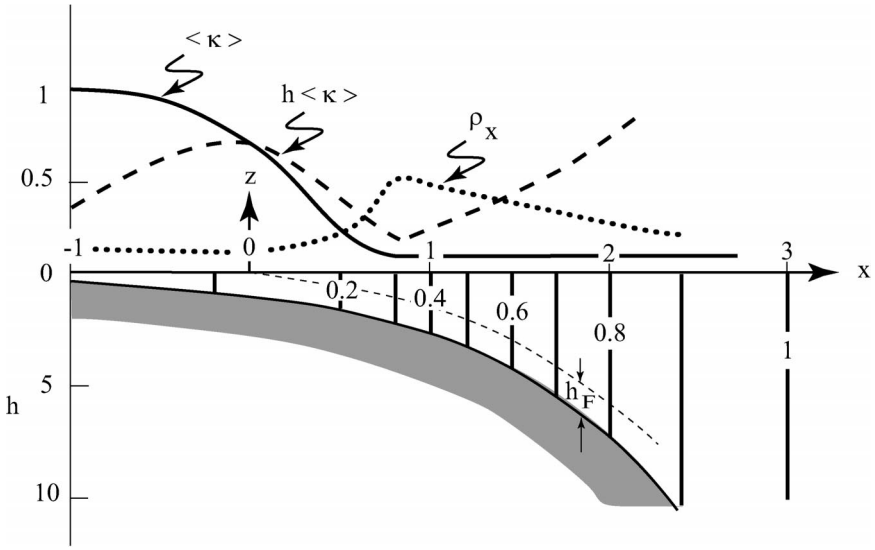

FIG. 2. The model domain for the analytical model, which consists of a cross-shore section of exponential bottom that is unvarying in the alongshore direction. All variables have been nondimensionalized as defined in the text. The solid line is the vertically averaged tidal diffusivity due to shear dispersion, which is merged with a background diffusivity set at 0.1. The dashed line is the vertically integrated (i.e., total) tidal diffusivity, which shows a local minimum at midshelf. The analytical solution is calculated for the case of a seaward Lagrangian transport of 0.2, and inshore and far-field boundaries set at $x = -1$ and 3, respectively. The density gradient is shown as the dotted line and isopycnals (vertical isopleths) are drawn in the water column. The thin dashed line marks the top of the tidal frictional layer. It is seen that the maximum density gradient is located at a water depth that is about twice this frictional depth.

in which primes and overbars denote the tidal and mean components respectively. Marking the vertical means by angle brackets and noting the definitions of the Stokes (Longuet-Higgins 1969) and Lagrangian velocities (subscripted S and L) as

$$(\overline{u'\eta'})_0 = h\langle\overline{u}_S\rangle, \quad \text{and} \tag{2.4}$$

$$\overline{u}_L = \overline{u} + \overline{u}_S, \tag{2.5}$$

Eq. (2.3) can be written as

$$(h\langle\overline{u}_L\rangle)_x = 0. \tag{2.6}$$

This equation states that the mean Lagrangian volume flux is constant in x, which is thus specified by its value at the inshore boundary, an external parameter of the model as discussed earlier.

We consider next the density equation of the form

$$\rho_t + (u\rho)_x + (w\rho)_z = (\nu\rho_z)_z, \tag{2.7}$$

where ν is the vertical diffusivity due to tides. Integrating this equation from the bottom to the surface and applying the kinematic and zero-flux conditions, one obtains

$$\partial_x \int_{-h}^{\eta} u\rho \, dz + \partial_t \int_{-h}^{\eta} \rho \, dz = 0. \tag{2.8}$$

This is the counterpart to (2.2) and can be similarly interpreted. If one takes the time mean of this equation and uses the Boussinesq approximation that

$$\rho' \ll \overline{\rho}, \tag{2.9}$$

one derives the counterpart to (2.3)

$$\partial_x\left[\int_{-h}^{0} (\overline{u}\,\overline{\rho} + \overline{u'\rho'}) \, dz + (\overline{u'\eta'}\,\overline{\rho})_0\right] = 0. \tag{2.10}$$

Defining the tidal diffusivity κ by

$$\overline{u'\rho'} = -\kappa\overline{\rho}_x \tag{2.11}$$

and recalling that $\overline{\rho}$ is constant in z, one may use (2.4) and (2.5) to reduce (2.10) to

$$\partial_x(h\langle\overline{u}_L\rangle\overline{\rho} - h\langle\kappa\rangle\overline{\rho}_x) = 0. \tag{2.12}$$

We have thus arrived at the equation governing the mean density, which states a balance between advection by the mean Lagrangian flow and the tidal diffusion.

It is important to note that although the vertical mixing may dominate the local balance to render the isopycnals vertical, it is the horizontal processes that determine the cross-shore distribution of density via (2.12). On the other hand, as discussed in the next section, tidal diffusivity is caused by vertical mixing (through shear dispersion), so the latter retains a central role in the model.

3. Hypothesis

Although a nonzero Lagrangian transport is included in the later derivation of the analytical solution, it is not

essential to our mechanism of frontogenesis, and hence is neglected for the following discussion. With this simplification, (2.12) can be integrated once to yield

$$-h\langle\kappa\rangle\overline{\rho}_x = F, \tag{3.1}$$

where F is an integration constant, which can be identified with the cross-shore buoyancy flux.

One notes from (3.1) that it is the vertically integrated (referred as ''total'') diffusivity $h\langle\kappa\rangle$—rather than the tidal diffusivity $\langle\kappa\rangle$—that determines the horizontal density gradient. Since the tidal diffusivity is expected to increase with the tidal amplitude—hence varying in the opposite sense from the water depth, one conceives the possibility that the total diffusivity may exhibit a minimum at mid shelf, which would imply via (3.1) a maximum in the density gradient. To assess this possibility, we next consider the spatial dependence of the tidal diffusivity.

4. Tidal diffusivity

As mentioned in the introduction, many processes may contribute to tidal diffusivity, including vertical- and horizontal-shear dispersion, and tidal random walk. Since the proposed frontogenesis hinges only on the gross depth dependence of the tidal diffusivity, it suffices for our purpose to use the one associated with vertical-shear dispersion. Additional reasons for this choice are that (i) it has been derived by Okubo (1967) based on first principles, thus containing fewer assumptions and (ii) unlike the other two processes, vertical-shear dispersion is operative in a two-dimensional numerical model used later to assess the analytical solution.

For his derivation, Okubo assumed a constant vertical diffusivity and a tidal velocity that varies linearly in the vertical. One of course may solve the tidal velocity explicitly (e.g., Loder 1980; Ou et al. 2000) to derive the resulting tidal diffusivity. The algebra however is complicated and deemed unnecessary for our purpose. In anticipation of later derivations, Okubo's expression of the tidal diffusivity is presented below in dimensionless units. Let T and U denote, respectively, the period and the amplitude of the cross-shore volume flux of the tide, we define the scale (indicated by brackets) for the depth by the frictional depth

$$[h] = (\nu T)^{1/2} \tag{4.1}$$

and for the tidal diffusivity by

$$[\kappa] = (240\nu)^{-1}U^2. \tag{4.2}$$

With the above scaling, his mean tidal diffusivity is given by

$$\langle\kappa\rangle = 30\pi^{-2}\tau^2\{1 - \tau[\coth(2\tau^{-1}) - \operatorname{csch}(2\tau^{-1})]\}, \tag{4.3}$$

where

$$\tau = h^{-2} \tag{4.4}$$

is an independent variable containing the depth dependence. With the cross-shore distance scaled by the e-folding distance L of the exponential bottom, this tidal diffusivity is plotted in Fig. 2 (the solid line), which is merged with a background diffusivity set at 0.1. It should be obvious from (3.1) that a nonzero background diffusivity is needed for the proposed frontogenesis, but the choice of this particular value will be discussed later (section 5).

It is seen that, as the bottom shoals, tidal diffusivity rises sharply as the frictional depth is approached and then levels off. The latter behavior is well known as the effectiveness of the shear dispersion is countered by enhanced vertical mixing (Geyer and Signell 1992). The drop-off of the tidal diffusivity beyond the unit depth is quite rapid, which can be seen from (4.3) to be given by

$$\langle\kappa\rangle \sim 30\pi^{-2}h^{-4} \quad \text{as } h \gg 1. \tag{4.5}$$

This power dependence can be crudely understood by first noting that tidal flux is quadratic in the tidal amplitude, which accounts for one-half of the power dependence; and the other two-quarters stem from the inverse depth-dependence of the tidal shear and the fractional depth occupied by the frictional layer.

Also plotted in Fig. 2 (the dashed line) is the total diffusivity, which is seen to exhibit a local minimum due to opposite trends in the tidal diffusivity and water depth. As argued in the previous section, such a minimum in the total diffusivity should yield a maximum in the density gradient; the rather robust nature of this minimum thus supports the proposed mechanism for frontogenesis. Moreover, this minimum is located where the tidal diffusivity merges with the background diffusivity, which, as can be seen from the figure, is not particularly sensitive to the magnitude of the latter so long as it is small. By setting (4.5) to the background value of 0.1, one obtains a depth of 2.3, in agreement with Fig. 2. Crudely, one thus expects the front, as defined by the maximum gradient, to be located at a water depth about twice the frictional depth. While this location is not sensitive to the magnitude of the background diffusivity, the frontal width can increase indefinitely if the latter goes to zero, underscoring its required finiteness as pointed out earlier (also discussed in section 7).

It is noted that, besides this local minimum at mid shelf, the total diffusivity also decreases toward the inshore boundary due to leveling of the tidal diffusivity as the bottom continues to shoal, which implies a sharpening gradient according to (3.1). One could argue, however, that the linear dynamics assumed by Okubo (1967) eventually breaks down when the water becomes too shallow, and so the tidal diffusivity may not actually level off. Moreover, as seen later, even a small offshore Lagrangian transport associated with land discharge effectively erases this feature, which thus should not be attached much significance.

5. Analytical solution

Having specified the tidal diffusivity, one may now solve (2.12) for density—expressed in terms of its anomaly denoted by ρ. Because of the constancy of the Lagrangian transport (2.6), this density anomaly is governed by the same equation, which can be nondimensionalized by $[\rho] = \Delta\rho$ (the total density range), and $[u_L] = [\kappa]L^{-1}$, in addition to the scaling rules defined earlier (section 4). Equation (2.12) remains unchanged by the nondimensionalization, which can be solved to yield

$$\rho_x = \frac{A}{h\langle\kappa\rangle}\exp\left(\int_0^x \frac{\langle\overline{u}_L\rangle}{\langle\kappa\rangle}\,dx\right), \tag{5.1}$$

and integrated once more to give

$$\rho = \frac{A}{h\langle\overline{u}_L\rangle}\exp\left(\int_0^x \frac{\langle\overline{u}_L\rangle}{\langle\kappa\rangle}\,dx\right) + B, \tag{5.2}$$

where A and B are integration constants, to be determined by the boundary conditions that ρ is zero at the inshore boundary and approaches unity in the far field, as defined by the scaling. For the analytical solution shown in Fig. 2, we set the inshore and offshore boundaries at $x = -1$ and 3, respectively, and use an offshore Lagrangian transport of 0.2 (its dimensional value is discussed in section 6).

It is seen that the density gradient indeed has a local maximum that is aligned with the minimum in the total diffusivity, as expected from (3.1). As alluded to earlier, the imposed Lagrangian transport has little effect on the midshelf front, but has largely eliminated the maximum gradient from the inshore boundary implied by (3.1). Although the frontal gradient is not particularly sharp, it does represent a significant enhancement from that of the surrounding water.

For a quantitative assessment of the solution, some dimensional values need to be assigned. Over the coastal region where tides are strong, the vertical diffusivity can be approximated by (Zimmerman 1986)

$$\nu \approx C_D U, \tag{5.3}$$

where C_D is the drag coefficient. The tidal strength, of course, varies widely over different coastal regions, and, as a plausible example, we set the vertically averaged cross-shore tidal velocity to be 1.5 m s^{-1} at 30-m isobath, which yields a cross-shore volume transport of about $U \approx 4.5 \times 10^5$ cm^2 s^{-1}. Tides of this magnitude are characteristic of a strong tidal regime, such as that encountered over Georges Bank, which will be referred to nonetheless as the ''standard'' case for convenience. If one uses 2×10^{-3} for the drag coefficient, one estimates a vertical diffusivity of $\nu \approx 0.9 \times 10^3$ cm^2 s^{-1}, and the scale for the tidal diffusivity $[\kappa] \approx 10^6$ cm^2 s^{-1}, both seem reasonable for Georges Bank (Yoshida and Oakey 1996; Loder et al. 1982; Houghton and Visbeck 1998). With the above estimates, the background diffusivity used in Fig. 2 has a dimensional value of 10^5 cm^2 s^{-1}. This diffusivity can be attained by a turbulent motion of 10 cm s^{-1} in velocity and 100 m in length scales, which are probably of the right orders of magnitude for a coastal ocean. In addition, the scale for the mean cross-shore velocity is 1 cm s^{-1}, so the Lagrangian transport used in Fig. 2 corresponds to an offshore velocity of only 0.2 cm s^{-1} where the water depth is the frictional depth. While this velocity is within the measurement error, it has largely eliminated the unrealistic gradient enhancement from the inshore boundary.

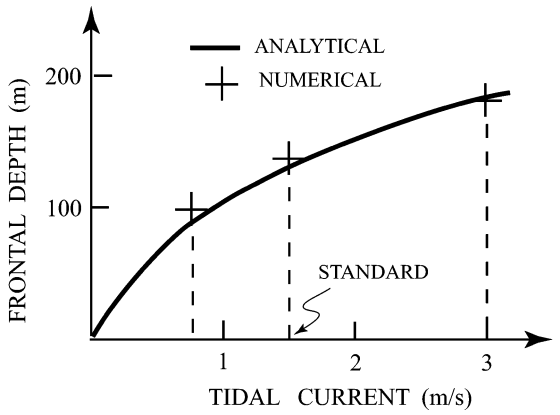

FIG. 3. The water depth of the front plotted as a function of the tidal amplitude—measured by the cross-shore tidal velocity at the 30-m isobath. The solid line represents that predicted by the analytical model, and the crosses mark that calculated from the numerical model.

Based on the above estimates, the frictional depth (4.1) is 62 m for the semidiurnal tide, so the front is located at a depth in excess of 100 m. Since this depth characterizes the shelf break off Georges Bank, one suspects that the type I front may not be distinguishable from the shelf-slope front. To facilitate further observational comparisons, we have plotted the predicted frontal depth in Fig. 3 (the solid line) as a function of the tidal amplitude—measured by the cross-shore tidal velocity at 30 m. It is seen that since the vertical diffusivity (5.3) is linear in the tidal amplitude, the frictional depth (4.1)—and hence the water depth where the front is located—varies as the square root of the tidal amplitude. In the shelf seas around the British Isles, one may use a tidal velocity one-half that of the standard case to yield a frontal depth of about 90 m, not unlike that observed by Hill and Simpson (1989). Over the continental shelves off the northeastern United States, the more appropriate tidal velocity is about one-quarter of the standard value (Beardsley et al. 1985), which implies a frontal depth of 60 m, not inconsistent with the observation of Ullman and Cornillon (2001).

The above square root dependence of the frontal depth on the tidal amplitude is much weaker than the cubic dependence entailed in the Simpson and Hunter (1974) criterion for a summer front, underscoring their fundamental difference. Although weak, the present functional dependence may nevertheless lead to detectable

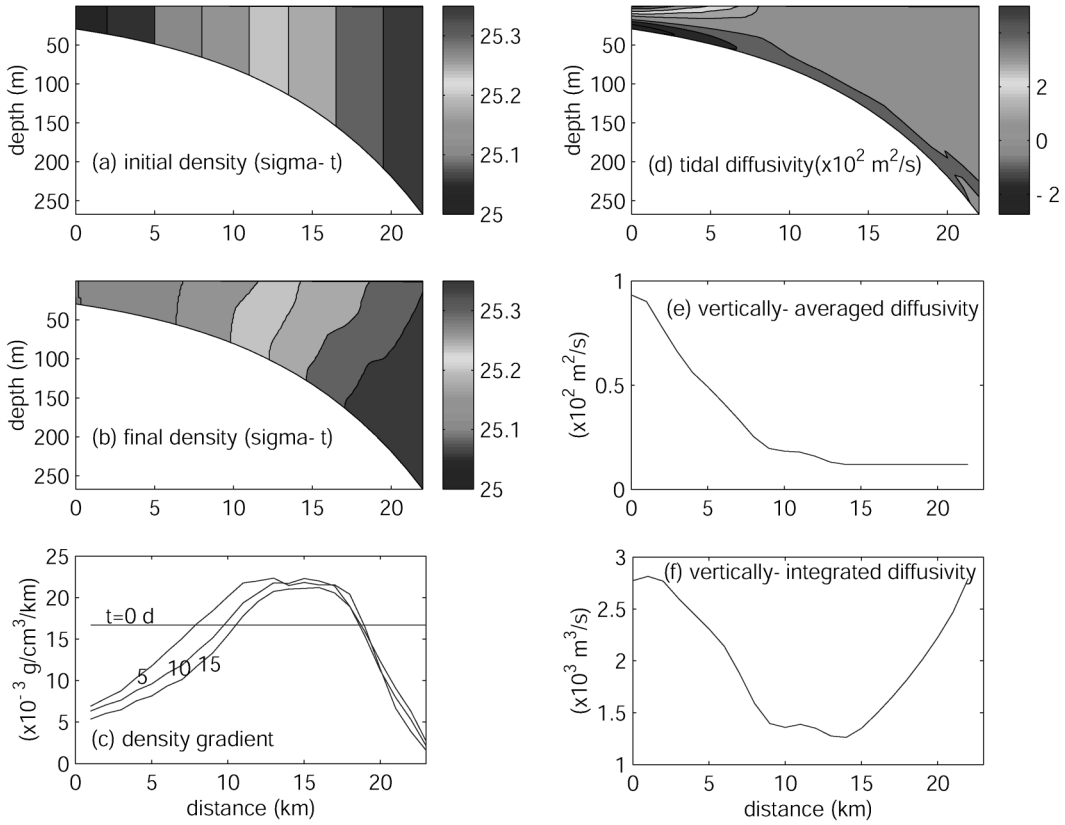

FIG. 4. Numerical calculations used to demonstrate the proposed frontogenesis, showing (a) the initial density field of uniform gradient, (b) the quasi-equilibrium state, and (c) the time evolution of the vertically averaged density gradient. Also shown are (d) the tidal diffusivity, calculated by dividing the tidal flux by the mean gradient; (e) its vertical average; and (f) its vertical integral. It is seen that the last has a minimum at midshelf where the maximum density gradient is located (c), in support of the analytical model.

frontal migration between spring and neap cycles. We have not yet found adequate data to assess this prediction.

6. Numerical solution

To test the analytical model, we carry out numerical calculations using the POM, a sigma-coordinate, free-surface, primitive equation model developed by Blumberg and Mellor (1987). The model is configured on the same cross-shore section as the analytical model, with the *e*-folding distance of the bottom set at 10 km (Fig. 4). Tides are imposed through a periodic surface displacement at the offshore edge, and the coastal buoyancy source is simulated by a specified density deficit relative to the offshore boundary. Sponge layers (20 km in width) are appended inside both these boundaries to damp out the reflected waves, and only solutions outside these layers are shown. There are 41 levels in the sigma coordinate, the horizontal grid spacing is 1 km, and the time interval for integration is 2 min.

For the solution shown in Fig. 4, we have used the parameter values similar to that of the standard case. Specifically, the amplitude of the surface displacement at the offshore boundary is set at 0.8 m so that the cross-shore tidal velocity is about 1.5 m s^{-1} at the 30-m isobath. The maximum alongshore tidal velocity turns out to be about 0.6 m s^{-1}, so tides are dominated by the cross-shore motion, as assumed in the analytical model. The total density range is set to 0.35 in the σ_t unit, and the model uses a background horizontal diffusivity of 10^5 cm^2 s^{-1}. To demonstrate more definitively the proposed frontogenesis, the initial density field (Fig. 4a) has a uniform cross-shore gradient. Following the initiation of the numerical integration, the (vertically averaged) density gradient begins to sharpen at midshelf at the expense of that of the surrounding water (Fig. 4c) and reaches a steady state after about 15 days, whose cross-shore distribution resembles the analytical curve (the dotted line in Fig. 2). The density lines at this quasi equilibrium are shown in Fig. 4b and are noticeably tilted, and so the assumption of vertical isopycnals used in the analytical model is not strictly satisfied. Nonetheless, the spacing of the density lines is similar to that shown in Fig. 2, underscoring the robustness of the basic physics, which transcends this assumption. Although the front is not particularly sharp in the contour plot (Fig. 4b), its gradient does represent a fivefold enhancement

from the surrounding value (Fig. 4c), and so the front is quite discernible.

For a further diagnosis of the numerical solution, we have plotted in Fig. 4d the tidal diffusivity, calculated by dividing the tidal flux by the mean gradient (2.11). At the grid points where the mean gradient is smaller than 10^{-3} g cm^{-3} km^{-1} or where the tidal diffusivity is smaller than the numerical diffusivity, the latter value is used in the contour plot. It should be emphasized that this tidal diffusivity is a calculated property, thus is distinct from—in fact can be an order of magnitude greater than—the explicit diffusivity used in the model. One notes first of all that the tidal diffusivity is highly heterogeneous in the vertical, even changing sign near the bottom (i.e., the tidal flux is countergradient)—a subject discussed in Ou et al. (2000). Since only the vertically averaged tidal diffusivity is relevant to our discussion, it is plotted in Fig. 4e, which tracks closely the solid curve shown in Fig. 2. This agreement suggests that tidal diffusion in the numerical model is indeed dominated by vertical-shear dispersion, the basis of the analytical curve. With this agreement, the total diffusivity, as plotted in Fig. 4f, then exhibits a minimum at midshelf, just as the dashed curve in Fig. 2. Since this minimum aligns with the gradient peak shown in Fig. 4c, we assert that the former is the cause of the model front, in support of the proposed diffusivity mechanism of frontogenesis.

For a further test of the predicted frontal depth shown in Fig. 3, we have carried out two more numerical runs by doubling and halving the tidal amplitude of the standard case. The numerical results are marked by crosses in the figure, which fall more or less on the analytical curve. This agreement provides a strong support of the analytical solution and, considering many differences of the numerical model, including how the vertical mixing is parameterized, it is somewhat surprising that the two models agree so closely.

7. Summary and discussion

We have proposed a mechanism of frontogenesis based on the varying strength of tidal mixing associated with depth change. It hinges on the fact that it is the vertically integrated (total) diffusivity, rather than the diffusivity itself, that determines the horizontal distribution of the property fields. Since tidal diffusivity increases with the tidal amplitude, and hence varies in the opposite sense from the water depth, the total diffusivity may exhibit a minimum at midshelf, which could yield a maximum in the property gradient—even in the absence of the flow convergence.

Because of generic depth dependence of the tidal diffusivity and the relative smallness of the background diffusivity, it is further deduced that the front is located where the water depth is about twice the tidal frictional depth, a prediction that is not inconsistent with some observed fronts. In a dramatic fashion, numerical calculations using the POM show the emergence of the front from an initial condition of uniform gradient. The diagnosis of the numerical solution through the calculation of the tidal diffusivity has supported the proposed frontogenesis mechanism, and the calculated frontal depth for different tidal amplitudes has further validated the analytical solution.

While the predicted location of front is quite robust, its sharpness—particularly on its seaward side—does vary with the background diffusivity, being more diffused if the latter is smaller. For the model solution shown, this background diffusivity is set to one tenth of the (maximum) tidal diffusivity, which, as seen earlier, is probably of the right order of magnitude for a coastal ocean. Although the model front is not particularly sharp, its gradient does represent a significant enhancement from the surrounding water and hence is quite discernible. In addition, other frontogenesis processes, such as geostrophic adjustment (Ou 1984), may act upon this nonuniformity in the density field to further sharpen its local gradient.

As the predicted frontal location is a property of the tides, one expects coincidental fronts for all passive properties—with the *same* gradient enhancement relative to their respective range. This is the reason that the front can be deciphered from, for example, temperature data (Ullman and Cornillon 2001) even though the salinity contrast dominates the density field. Moreover, one need not be specific about the source of a particular property contrast—the reason that the model can be applied to Georges Bank even though the salinity signal there is not directly linked to the local discharge. Since the frictional depth is defined for a particular tidal constituent, there exist in principle spatially separated fronts associated with other tidal constituents, which, however, may not be discernible given the dominance of the semidiurnal tides.

Although the model is concerned with the tidal front, a similar hypothesis can be formulated for the shelfbreak front. Instead of tidal mixing, one invokes wind- and cooling-induced mixing, which is more vigorous over the shelf, and beyond the shelf break, there is again an increase in total diffusivity due to rapidly increasing water depth and its possible enhancement by mesoscale eddies. That is, there could very well be a minimum in the total diffusivity at the shelf break, and hence a front. Since these mixing processes are less deterministic than tidal mixing, the model formulation obviously requires more substantiation. It nonetheless may provide an alternative explanation of the shelfbreak front that is based on cross-shore balances—in contrast to its depiction as a three-dimensional feature that emerges gradually along-shore (Gawarkiewicz and Chapman 1992; Chapman 2000).

Acknowledgments. The work is supported by the National Science Foundation through Grant ATM-96-

18260. We thank the anonymous reviewers, whose comments have led to significant improvement of the paper.

REFERENCES

Beardsley, R. C., D. C. Chapman, K. H. Brink, S. R. Ramp, and R. Schlitz, 1985: The Nantucket Shoals Flux Experiment (NSFE79). Part I: A basic description of the current and temperature variability. *J. Phys. Oceanogr.*, **15,** 713–748.

Blumberg, A. F., and G. L. Mellor, 1987: A description of a three-dimensional coastal ocean model. *Three-Dimensional Coastal Ocean Models,* N. Heaps, Ed., Vol. 4, Amer. Geophys. Union, 1–16.

Chapman, D. C., 2000: Boundary layer control of buoyant coastal currents and the establishment of a shelfbreak front. *J. Phys. Oceanogr.*, **30,** 2941–2955.

Fedorov, K. N., 1983: *The Physical Nature and Structure of Oceanic Fronts.* Lecture Notes on Coastal and Estuarine Studies, Springer-Verlag, 333 pp.

Fisher, H. B., E. J. List, R. C. Y. Koh, J. Imberger, and N. H. Brooks, 1979: *Mixing in Inland and Coastal Waters.* Academic Press, 483 pp.

Garvine, R. W., 1995: A dynamical system for classifying buoyant coastal discharges. *Cont. Shelf Res.*, **15,** 1585–1596.

Gawarkiewicz, G., and D. C. Chapman, 1992: The role of stratification in the formation and maintenance of shelf-break fronts. *J. Phys. Oceanogr.*, **22,** 753–772.

Geyer, W. R., and R. P. Signell, 1992: A reassessment of the role of tidal dispersion in estuaries and bays. *Estuaries,* **15,** 97–108.

Hickox, R., I. Belkin, P. Cornillon, and Z. Shan, 2000: Climatology and seasonal variability of ocean fronts in the East China, Yellow and Bohai seas from satellite SST data. *Geophys. Res. Lett.*, **27,** 2945–2948.

Hill, A. E., and J. H. Simpson, 1989: On the interaction of thermal and haline fronts. The Islay front revisited. *Estuarine Coast. Shelf Sci.*, **28,** 495–505.

Hoskins, B. J., and F. P. Bretherton, 1972: Atmospheric frontogenesis models: Mathematical formulation and solution. *J. Atmos. Sci.*, **29,** 11–37.

Houghton, R. W., and M. Visbeck, 1998: Upwelling and convergence in the Middle Atlantic Bight shelfbreak front. *Geophys. Res. Lett.*, **25,** 2765–2768.

Loder, J. W., 1980: Topographic rectification of tidal currents on the sides of Georges Bank. *J. Phys. Oceanogr.*, **10,** 1399–1416.

——, D. G. Wright, C. Garrett, and B.-A. Juszko, 1982: Horizontal exchange on central Georges Bank. *Can. J. Fish. Aqua. Sci.*, **39,** 1130–1137.

Longuet-Higgins, M. S., 1969: On the transport of mass by time-varying ocean currents. *Deep-Sea Res.*, **16,** 431–447.

Okubo, A., 1967: The effect of shear in an oscillatory current on horizontal diffusion from an instantaneous source. *Int. J. Oceanol. Limnol.*, **1,** 194–204.

Ou, H. W., 1984: Geostrophic adjustment: A mechanism for frontogenesis. *J. Phys. Oceanogr.*, **14,** 994–1000.

——, C. Dong, and D. Chen, 2000: On the tide-induced property flux: Can it be locally counter-gradient? *J. Phys. Oceanogr.*, **30,** 1472–1477.

Simpson, J. H., and J. R. Hunter, 1974: Fronts in the Irish Sea. *Nature,* **250,** 404–406.

Taylor, G. I., 1953: Dispersion of soluble matter in solvent flowing slowly through a tube. *Proc. Roy. Soc. London,* **A219,** 186–203.

Ullman, D. S., and P. C. Cornillon, 2001: Continental shelf surface thermal fronts in winter off the northeast US coast. *Cont. Shelf Res.*, **21,** 1139–1156.

Yoshida, J., and N. S. Oakey, 1996: Characterization of vertical mixing at a tidal-front on the Georges Bank. *Deep-Sea Res.*, **43B,** 1713–1744.

Zimmerman, J. T. F., 1986: The tidal whirlpool: A review of horizontal dispersion by tidal and residual currents. *Netherland. J. Sea. Res.*, **20,** 133–154.